Published in final edited form as:
Nat Immunol. 2016 October ; 17(10): 1206–1215. doi:10.1038/ni.3537.

Foxn1 regulates key target genes essential for T cell development in postnatal thymic epithelial cells

Saulius Žuklys[#1,*], **Adam Handel**[#2], **Saule Zhanybekova**[#¶], **Fatima Govani**[3], **Marcel Keller**[1,°], **Stefano Maio**[3], **Carlos E. Mayer**[1], **Hong Ying Teh**[1], **Katrin Hafen**[1], **Giuseppe Gallone**[2], **Thomas Barthlott**[1], **Chris P. Ponting**[2,§], and **Georg A. Holländer**[1,3,*]

[1]Department of Biomedicine, University Children's Hospital and University of Basel, Basel, Switzerland [2]MRC Functional Genomics Unit, Department of Physiology, Anatomy and Genetics, University of Oxford, Oxford, United Kingdom [3]Department of Paediatrics and the Weatherall Institute of Molecular Medicine, University of Oxford, Oxford, United Kingdom

[#] These authors contributed equally to this work.

Abstract

Thymic epithelial cell differentiation, growth and function depend on the expression of the transcription factor Foxn1, however its target genes have never been physically identified. Using novel static and inducible genetic model systems and chromatin studies, we provide now a genome wide map of direct Foxn1 target genes for postnatal thymic epithelia and define the Foxn1 binding motif. We detail the function of Foxn1 in these cells and demonstrate that in addition to the transcriptional control of genes involved in the attraction and lineage commitment of T cell precursors, Foxn1 regulates the expression of genes involved in antigen processing and thymocyte selection. Thus, critical events in thymic lympho-stromal cross-talk and T cell selection are indispensably choreographed by Foxn1.

The thymic microenvironment is unique in its ability to promote the development and selection of naïve T cells with a repertoire purged of vital "self" specificities but prepared to react to injurious "non-self". Thymic epithelial cells (TEC), which can be categorized into separate cortical (cTEC) and medullary (mTEC) lineages1,2, are essential for this

[*]Correspondence should be addressed to G. A. H. at georg.hollander@paediatrics.ox. ac.uk or S.Z. at saulius.zuklys@unibas.ch.
[°]Present address: Actelion Pharmaceuticals Ltd, 4123 Allschwil, Switzerland
[§]Present address: MRC Institute of Genetics and Molecular Medicine, University of Edinburgh, United Kingdom
[¶]Present address: Department of Chemistry, University of Basel, Basel, Switzerland

Accession codes.
GSE75219

Author contributions
S.Z., S.Zh., A.H. and G.A.H. designed the experiments. S.Z., C.E.M., S.Zh., H.Y.T., K.H., S.M. and M.K. performed the experiments. S.Z., A.H., S.Zh., C.E.M., T.B., G.G., C.P.P. and G.A.H. analyzed and/or interpreted the results. G.A.H. wrote the manuscript with contributions from A.H. and S.Z..

Competing financial interests
The authors declare no competing financial interests.

competence. cTEC attract blood-borne precursor cells, commit them to a T cell fate and foster their differentiation to express an αβT cell antigen receptor (TCR). Reactivity to major histocompatibility complex (MHC)-peptide complexes presented by TEC authorizes the generation of a bespoke TCR repertoire. Because TCR are initially generated pseudo-randomly, their specificity is scrutinized during thymocyte development to establish a selected repertoire tailored for an individual whereby cTEC positively select thymocytes that express a TCR of sufficient affinity for self-antigens3. Subsequently, both cTEC and mTEC deplete thymocytes with significant reactivity to self-antigens, a process known as negative selection4.

TEC differentiation and growth are dependent on transcription factor Foxn1 which is present in the thymus exclusively in TEC but not required there for the cells' initial fate specification5,6,7. *Foxn1* is continuously expressed in the thymus and may therefore be required for the maintenance of cortical and medullary TEC, both in the embryo and in postnatal mice8–10. This finding suggests that *Foxn1* constantly controls diverse aspects of TEC biology, ranging from steps essential in early epithelial cell differentiation to the transcriptional control of genes important for thymus function and maintenance. Though several genes have been implicated to be transcriptionally controlled by Foxn1, none have physically been identified as direct targets. Using different static and inducible genetic mouse model systems, we now demonstrate in a genome wide manner the direct target genes of Foxn1. Among these are genes that contribute to antigen processing and presentation including threonine peptidases, components of the proteasome complex, protein transporters and CD83.

Results

A Foxn1 transgenic rescue of the nude thymus phenotype

The direct identification of Foxn1 target genes in TEC using chromatin immunoprecipitation sequencing (ChIP-seq) is impeded by a lack of suitable anti-Foxn1 antibodies. We therefore generated nude ($Foxn1^{nu/nu}$) mice transgenic for a BAC11 that encodes a Foxn1 protein tagged with a Flag-octapeptide which is expressed under the normal control of *Foxn1* regulatory elements and permits immunoprecipitation (Supplementary Fig. 1a,b). Homozygous for the BAC, these mice (designated $Foxn1^{wt*/wt*}$) had a regular coat and a gross anatomically normal thymus with an ordered stromal architecture and usual Foxn1 protein expression. Total thymus and TEC cellularity were mildly reduced in mice 4 weeks or older when compared to age-matched wild type controls (Fig. 1a and Supplementary Fig. 1c,f). Hence, the Foxn1-Flag protein in TEC of $Foxn1^{wt*/wt*}$ mice almost completely rescued the nude phenotype. In contrast to $Foxn1^{wt*/wt*}$ mice, nude mice heterozygous for the BAC allele (designated $Foxn1^{wt*/-}$) had a significantly smaller thymus marked by reduced Foxn1 protein expression, fewer mTEC, multiple large cysts and a severely disorganized cortex-medulla segregation with medullary islands located adjacent to the organ's capsule (Fig. 1a-e and Supplementary Fig. 1c,f). Furthermore, $Foxn1^{wt*/-}$ mice had fewer mature ($MHC^{hi}CD80^{+}CD86^{+}$) mTEC and their MHCII cell surface expression was reduced in comparison to wild type and $Foxn1^{wt*/wt*}$ mice (Fig. 1f-h). These results

therefore established the recombinant BAC as hypomorphic *Foxn1* allele with expression of Foxn1-Flag from a single allele only partially rescuing the nude thymus phenotype.

Foxn1 acts at multiple stages of thymocyte differentiation and selection

We next evaluated the thymopoiesis of 4-6 week old Foxn1$^{wt*/wt*}$, Foxn1$^{wt*/-}$ and wild type mice. The progression of early thymic precursors (ETP, which are Lin$^-$CD4$^-$CD8$^-$CD44$^+$c-kit$^+$ thymocytes, whereby lineage negativity, Lin$^-$, refers to the absence of TCRβ, CD4, CD8, CD19, CD11c, CD11b, F4/80, TCRγδ, NK1.1, and TER119 expression) to CD4$^+$CD8$^+$ (double positive, DP) thymocytes was comparable for Foxn1$^{wt*/wt*}$ and wild type mice (Fig. 2a-c), indicating that homozygous BAC transgene rescued the early thymopoietic competence of *Foxn1*$^{nu/nu}$ TEC. In contrast, the frequency of ETP, a population that seeds the thymus in response to chemokines CCL19, CCL21 and CCL25 expressed by TEC12, was 32-fold reduced in Foxn1$^{wt*/-}$ mice (Fig. 2a) whilst B cells were 30-fold more frequent in Foxn1$^{wt*/-}$ mice relative to wild type animals (Supplementary Fig. 2a). The frequency of the subsequent stages of Lin- thymocytes increased in Foxn1$^{wt*/-}$ mice relative to ETP but did not reach the values observed in wild type animals (Fig. 2b).

The frequency of mature CD4$^+$ single-positive (CD4SP) and CD8$^+$ single-positive (CD8SP) thymocytes was mildly reduced in Foxn1$^{wt*/wt*}$ and strongly diminished in Foxn1$^{wt*/-}$ mice when compared to wild type animals (Fig. 2c). These changes in Foxn1$^{wt*/wt*}$ and Foxn1$^{wt*/-}$ mice correlated with a reduced positive selection as measured by the upregulation of CD69 expression on thymocytes with an intermediate expression of the TCR despite an increased frequency of cTEC relative to that observed in wild type mice (Fig. 1e, Fig. 2d and Supplementary Fig. 2b). Because a decrease in CD4SP and CD8SP thymocytes could also be the consequence of increased clonal deletion, we next determined among cortical TCR^{hi} DP thymocytes the frequency of negatively selected thymocytes marked by co-expression of PD1 and Helios in the absence Foxp3 and CCR7.13,14 Their frequency was diminished in both Foxn1$^{wt*/wt*}$ and Foxn1$^{wt*/-}$ mice in comparison to wild type animals (Fig. 2e).

We next investigated the post-selection maturation of medullary thymocytes. The up-regulation of CCR7 on CD4SP thymocytes was reduced in Foxn1$^{wt*/-}$ mice (Fig. 2f) whereas the expression of Helios, a marker identifying cells undergoing Bim-mediated negative selection14, was at initial stages diminished but increased at later stages during maturation in Foxn1$^{wt*/-}$ mice relative to wild type mice (Fig. 2f), revealing increased negative selection of these cells. Medullary CD8SP thymocytes demonstrated in Foxn1$^{wt*/-}$ mice a decreased down-regulation of CD24, thus also revealing a partial block in maturation (Fig. 2g). Moreover, the differentiation of immature and mature regulatory T cells (T_{reg} cells) was also diminished in Foxn1$^{wt*/wt*}$ and Foxn1$^{wt*/-}$ mice when compared to wild type animals (Fig. 2h and Supplementary Fig. 2c). Hence, an incomplete complementation of Foxn1 altered T cell development marked by a lower frequency of ETP, reduced positive selection, partial maturational blocks and a variance in negative thymocyte selection that resulted in fewer mature, post-selection thymocytes.

Identification of Foxn1 binding sites and motifs

ChIP-seq analyses employing a Flag-tag specific antibody (Supplementary Fig. 3a) and TEC nuclear extracts from Foxn1$^{wt*/wt*}$ mice identified 9,012 peaks at an irreproducible discovery rate (IDR) of < 0.05. A third of these peaks were located immediately 5' and within 5kb upstream of transcriptional start sites (TSS) (Fig. 3a,b). Overlap of these peaks with H3K4me3 marks was enriched approximately 23-fold (Supplementary Fig. 3b) and 75-fold enhanced within open chromatin regions, as measured by ATAC-seq in cTEC (Fig. 3b). Approximately two-thirds (67.3%) of Foxn1 binding sites intersected ATAC-seq peaks and this value increased to 92.8% when considering only binding sites within regions 5kb upstream and 100 bases downstream of the transcriptional start sites (TSS) of genes. In contrast, Foxn1 showed a 0.53-fold reduction ($p<0.0001$) in binding near the TSS of genes encoding tissue restricted antigens relative to all others15.

Using a non-supervised method on all Foxn1 ChIP-seq peaks with an IDR<0.05, we identified, based on our results, a consensus Foxn1 binding motif of 5 nucleotides (GA-a/c-GC) (Supplementary Fig. 3c,d). Focusing our analysis on peaks within 5kb upstream and 100 bases downstream of the TSS refined the prediction of the Foxn1 binding motif to GACGC (Fig. 3c). This motif was associated with a higher binding affinity across all peaks, even after adjustment for GC content (GACGC: $\beta = 6.1$, $p<0.0001$; GAAGC: $\beta = -0.8$, $p = 0.44$) and was strongly enriched (3.2-fold) around the summit of Foxn1 ChIP-seq peaks when compared to surrounding sequences (Fig. 3d). This Foxn1 core binding sequence is identical to a previously suggested motif found by *in vitro* studies16, further indicating the validity of our ChIP-seq analysis using primary TEC. Taken together, these results identified the Foxn1 core binding motif within regions of open chromatin in TEC and near the TSS.

Identification of Foxn1 target genes

Because transcription factor binding does not necessarily result in the transcriptional regulation of nearby genes, we analyzed the gene expression profiles of cTEC and mTEC isolated by FACS from 1 week old Foxn1$^{wt*/wt*}$ and Foxn1$^{wt*/-}$ mice, respectively (Supplementary Fig. 4a,b). Large numbers (8378 and 11690, respectively) of genes were differentially expressed in cTEC and mTEC of Foxn1$^{wt*/-}$ relative to Foxn1$^{wt*/wt*}$ mice (Supplementary Table 1) with the TEC transcriptional profiles of Foxn1$^{wt*/wt*}$ mice highly correlating with previously published data of wild type TEC15 (mean ± SD Spearman's r - cTEC: 0.94 ± 0.00; mTEC: 0.92 ± 0.00).

To address the issue which of the TEC transcriptomic differences observed in Foxn1$^{wt*/-}$ mice are the consequence of a change in direct Foxn1-mediated gene regulation, we generated triple mutant mice (*Psmb11-rtTA::tetO-Cre::Foxn1$^{7,8loxP/loxP}$*), designated iFoxn1$^{\Delta 7,8}$, in which exons 7 and 8 of the *Foxn1* locus can be deleted in a doxycyclin (Dox)-induced, cTEC-restricted fashion (Supplementary Fig. 5a-c). The thymi of these mice displayed in the absence of Dox treatment a regular architecture, epithelial composition and lymphopoietic function (Supplementary Fig. 6 and data not shown). Three days after Dox exposure, the thymus of these mice had largely lost Foxn1 expression (Supplementary Fig. 6a) and displayed a decreased cellularity despite normal intrathymic T cell development, as assessed by CD4 and CD8 expression (Supplementary Fig. 6b,c). However, there was a

severe decrease in $CD44^{+}CD25^{+}CD4^{-}CD8^{-}Lin^{-}$ and $CD44^{-}CD25^{+}CD4^{-}CD8^{-}Lin^{-}$ thymocytes when comparing 3-day Dox-treated with untreated $iFoxn1^{\Delta7,8}$ mice (Fig. 4a). These results therefore demonstrated that continuous and steady state Foxn1 expression in postnatal cTECs is required for normal T cell development.

Transcriptome analysis of cTEC from 1 week old $iFoxn1^{\Delta7,8}$ mice isolated 3 days after Dox treatment identified 2506 differentially regulated genes compared to cTEC isolated from Dox treated $iFoxn1^{\Delta7,8}$ mice deficient for the *TetO-Cre* transgene and thus unresponsive to Dox (FDR<0.05) (Supplementary Table 1, Supplementary Fig. 4c). Many of the down-regulated genes (566) most likely represented direct targets because their Foxn1 binding sites were placed within 5kb upstream and 100 bases downstream of their TSS and their transcripts decreased coincidental with a loss of full length *Foxn1* transcripts, as demonstrated for several previously suspected Foxn1 target genes essential for early thymocyte development, including *Ccl25*12, *Cxcl12*17 and *Dll4*18 (Fig. 4b). Samples from $Foxn1^{wt*/wt*}$ and $Foxn1^{wt*/-}$ mice segregated in principal component analysis first by cell type and then by genotype (Supplementary Fig. 7a) and samples from $iFoxn1^{\Delta7,8}$ mice separated in this analysis according to the presence or absence of the *TetO-Cre* transgene (Supplementary Fig. 7b). These observations therefore supported the validity of the mouse model to probe Foxn1 biology.

We next integrated the Foxn1 ChIP-seq data with TEC RNA-seq data from $Foxn1^{wt*/wt*}$, $Foxn1^{wt*/-}$ and $iFoxn1^{\Delta7,8}$ mice. This enabled us to identify a set of high confidence genes both directly bound and transcriptionally regulated by Foxn1. 5,415 genes were identified by ChIP-seq that had Foxn1 peaks within 5kb upstream or 100 bases downstream of the TSS (Fig. 4c). Of these, 1749 genes contained at least one Foxn1 binding peak and were up-regulated in TEC of $Foxn1^{wt*/wt*}$ relative to $Foxn1^{wt*/-}$ mice (Fig. 4c). Finally, 450 of the 1148 genes bound by Foxn1 and up-regulated in cTEC of $Foxn1^{wt*/wt*}$ relative to $Foxn1^{wt*/-}$ mice were also up-regulated in $iFoxn1^{\Delta7,8}$ mice that lacked the *TetO-Cre* transgene in comparison to $iFoxn1^{\Delta7,8}$ mice able to delete *Foxn1* in response to Dox treatment (Fig. 4c, Table 1 and Supplementary Table 2). Using the binding and expression target analysis (BETA) software package on our ChIP-seq and cTEC transcriptomic data indicated that Foxn1 functioned predominantly as a transcriptional activator ($p < 10^{-7}$)19 because Foxn1 ChIP-seq peaks were 1.92-fold more likely (p<0.01) to mark genes whose expression was decreased in cTEC of $iFoxn1^{\Delta7,8}$ mice in which *Foxn1* had been deleted (Fig. 4d; Supplementary Fig. 8).

We next identified Foxn1 ChIP-seq peaks of cTEC genes that were placed near TSS and intersected an ATAC-seq peak, and compared those to ChIP-seq peaks that did not have such an association. There was no significant difference in the $\log_2$ fold change of gene expression between cTEC from $iFoxn1^{\Delta7,8}$ mice or $iFoxn1^{\Delta7,8}$ mice that lacked the *TetO-Cre* transgene (p=0.14). However, the presence of an ATAC-seq peak in cTEC was predictive in $iFoxn1^{\Delta7,8}$ mice of the magnitude of expression for genes with a nearby Foxn1 ChIP-seq peak (ATAC-seq peak *vs.* no ATAC-seq peak: 2.4-fold, p<0.0001).

The high confidence Foxn1 gene targets we had identified demonstrated a higher median chromatin accessibility in cTEC when compared to all other genes (p<0.0001; Fig. 4e).

mRNA expression from high confidence genes showed a significant linear relationship with the relative proportion of full-length, wild type *Foxn1* transcripts in iFoxn1$^{\Delta 7,8}$ mice (Supplementary Fig. 9). Most of these high confidence Foxn1 targets were highly expressed in cTEC of Foxn1$^{wt*/wt*}$ mice (FPKM > 10: 360 genes), although many of them were also expressed in mTEC of Foxn1$^{wt*/wt*}$ mice (FPKM > 1: 428 genes; Fig. 4f), suggesting that our approach identified genes of importance to general TEC biology. To check that these high confidence Foxn1 targets were not driven by contamination with other thymic stromal cells, we screened the Foxn1 target genes identified in TEC against a list of potential contaminants derived from a previous microarray study of cell types resident in the thymus.[22,23] None of the high confidence Foxn1 targets were identified as being derived from contaminating cell types.

We next assessed whether the comparison between cTEC from Foxn1$^{wt*/wt*}$ and Foxn1$^{wt*/-}$ mice captured similar underlying transcriptomic changes as was observed for cTEC from Dox-treated iFoxn1$^{\Delta 7,8}$ mice when compared to cTEC from Dox-treated iFoxn1$^{\Delta 7,8}$ mice lacking the *TetO-Cre* transgene. The direction of overall expression changes in the two models showed a modest agreement (Spearman's r = 0.46, p<0.0001). When restricting this analysis only to genes that were significant (FDR < 0.05) in both models, the agreement was more marked (Spearman's r = 0.81, p<0.0001; Supplementary Fig. 10), suggesting that the models were capturing aspects of the same underlying biological processes and that the ability to identify and validate genes potentially regulated by Foxn1 was enhanced by the intersection of these two datasets. We have therefore employed ChIP-seq and RNA-seq datasets to identify a core set of 450 high confidence Foxn1 target genes.

Foxn1 targets are associated with antigen processing and presentation

We used gene ontology analysis[20] to identify the biological categories to which high confidence Foxn1 target genes contribute. A significant enrichment was observed for categories involving threonine peptidases including *Tasp1,* the_components of the proteasome complex, such as *Psmb9*, *Psmb10*, *Psmb4* and *Psma4* (16.7-fold and 7.29-fold respectively; p<0.0001; Fig. 4g and Supplementary Table 3) and protein transporters including *Tap2* required for antigen presentation by MHCI. In addition, we identified the expression of *Prss16,* which encodes a thymus specific serine protease expressed in cTEC and required for CD4 lineage selection and high MHCII expression[21], to be regulated by Foxn1 (Table 1). Thus, Foxn1 controls multiple mechanisms critical for self-antigen processing and presentation.

Given this significant association of *Foxn1* expression with pathways involved in antigen presentation, we next tested whether there was a differential expression of Aire-regulated genes between mTEC of Foxn1$^{wt*/wt*}$ and Foxn1$^{wt*/-}$ mice. As a group, Aire-regulated genes tended to be more highly expressed in mTEC of Foxn1$^{wt*/wt*}$ than Foxn1$^{wt*/-}$ mice when compared to either Aire-independent tissue restricted antigens or all other protein-coding genes (median fold change: *Aire*-induced tissue restricted antigens 2.93-fold, other *Aire*-induced genes 2.61-fold, *Aire*-independent tissue restricted antigens 1.14-fold, and other protein-coding genes 1.00-fold; p<0.05 for all pair-wise comparisons). As *Aire* expression was comparable in mTEC of Foxn1$^{wt*/wt*}$ and Foxn1$^{wt*/-}$ mice (1.10-fold,

p=0.23), these findings suggest that Foxn1 expression facilitates promiscuous gene expression in a fashion that is independent but complementary to Aire.

We then used existing TEC transcriptomic datasets to place our high-confidence Foxn1 targets in the context of a cTEC-specific co-expression network constructed using microarray data generated at multiple developmental time points22,23. We used weighted gene co-expression network analysis to identify gene modules containing more Foxn1 targets than expected by chance (Supplementary Fig. 11; Supplementary Table 4). *Dll4*, *Ccl25* and several other putative high confidence Foxn1 targets were significantly enriched within a gene module associated with the regulation of T cell activity (Supplementary Table 4). The high confidence Foxn1 targets formed in cTEC a biological coexpression network ($p<0.002$) where Foxn1 represented a highly connected central hub (Supplementary Fig. 12a). Hence, Foxn1 target genes formed an interconnected co-expression hub associated with antigen processing and presentation.

Identification of Foxn1 co-factors

To identify DNA binding factors that could cooperate with Foxn1 in controlling gene expression, we next searched for known transcription factor recognition motifs within and adjacent to Foxn1 ChIP-seq peaks. This analysis identified several motifs that were significantly and centrally overrepresented when compared to a background of mixed promoter and enhancer regions (Supplementary Fig. 12b,c)24. Among these were binding sites for the transcription factors CREB1 and TP63, which are known to regulate proliferation and TEC aging, respectively25,26. Foxn1 binding in TEC was 11.7-fold enriched near TP63 binding sites previously recognized in *Foxn1* expressing keratinocytes ($p < 0.0001$), supporting a Foxn1-TP63 axis regulating TEC homeostasis26,27. We thus identified a number of potential Foxn1 co-factors, of which TP63 is a particularly biologically plausible candidate.

Psmb11 and *Cd83* are direct Foxn1 targets

Psmb11, encoding the proteasome component β5t, and *Cd83* were identified as two high confidence Foxn1 target genes (Table 1). As early as 24 hours post-Dox treatment, transcripts for both genes were significantly reduced in cTEC from iFoxn1$^{\Delta 7,8}$ mice when compared to untreated iFoxn1$^{\Delta 7,8}$ mice (Fig. 5a), suggesting the genes' direct transcriptional control by Foxn1. *Psmb11* is expressed almost exclusively in cTECs and is pivotal for positive selection of CD8^{+} T cells28,29. CD83 is a surface marker expressed in cTEC that is required for the development of CD4SP cells.30 A single Foxn1 binding peak was identified upstream of *Psmb11*'s TSS that contained two copies of the Foxn1 binding motif GACGC and two copies of the predicted alternative motif GAAGC. The *Cd83* promoter contained a proximal GACGC and three distal GAAGC motifs (Fig. 5a). The functional significance of these binding sites was investigated in HEK293 cells co-transfected with a *Foxn1* expression plasmid and a luciferase construct containing the *Psmb11* and the *Cd83* promoter, respectively, each without or with disrupted consensus motifs. Mutations of the proximal and, to a lesser degree, distal GACGC motifs of the *Psmb11* promoter significantly decreased luciferase activity, whereas changes to both ablated transcription altogether (Fig. 5b). Deletion of the single GACGC motif in the promoter of *Cd83* decreased the

transcriptional activity by half and removal of the promoter sequence containing the distal two GAAGC motifs reduced transcription by two-thirds (Fig. 5c). Mutating the proximal GAAGC in the truncated promoter, in contrast to removal of GACGC, had no effect on the transcriptional activity (Fig. 5c). Thus, the provision of Foxn1 in heterologous HEK293 cells is sufficient to activate the minimal *Psmb11 and Cd83* promoters, each containing intact GACGC Foxn1 binding motifs.

In comparison to wild type animals, Foxn1$^{wt*/-}$ mice had 4-fold fewer CD8SP thymocytes (Fig. 5d), which correlated with a partial block in thymocyte selection, as measured by CD69 and TCR surface expression (Fig. 5e). These changes closely but not completely mirrored those observed in *Psmb11*-deficient mice (Fig. 5d,e). We therefore investigated the negative selection of cortical (i.e. CCR7^{-}) DP thymocytes as marked by their simultaneous expression of PD-1 and Helios.14 In contrast to wild type but similar to *Psmb11*$^{-/-}$ mice, the frequency of PD1^{+}Helios^{+} DP thymoyctes was reduced by half in Foxn1$^{wt*/-}$ animals (Fig. 5f), suggesting a compromised negative thymocyte selection in the absence of normal *Foxn1* complementation and thus regular *Psmb11* expression. Identical to *Psmb11*$^{-/-}$ mice, Foxn1$^{wt*/-}$ animals, in contrast to wild type mice, had also 4-fold fewer TCR^{hi}CD5^{int} DP thymocytes (Fig. 5g), a population representing CD8 lineage committed DP thymocytes.31 CD8SP thymocytes of both Foxn1$^{wt*/-}$ and *Psmb11*$^{-/-}$ mice exhibited a reduced downregulation of CCR7 and CD24 expression when compared to wild type animals (Fig. 5h), revealing a block in thymocyte maturation at the post-selection stage. A loss in regular Foxn1 expression in Foxn1$^{wt*/-}$ mice resulted in decreased β5t expression (Supplementary Fig. 13) and, consequently, a loss in regular thymocyte differentiation at consecutive stages along the CD8SP lineage.

cTEC of Foxn1$^{wt*/-}$ mice had practically lost their CD83 expression (Fig. 6a). This resulted in 4-fold fewer CD4SP thymocytes relative to wild type animals, a decline that was significantly bigger than that observed in CD83 deficient (*Cd83*$^{-/-}$) mice (Fig. 6b). Positive selection of DP thymoyctes, as assessed by CD69 and TCR expression, was also significantly lower in Foxn1$^{wt*/-}$ mice compared to *Cd83*$^{-/-}$ animals (Fig. 6c), suggesting Foxn1-dependent mechanisms other than CD83 expression to be required for positive selection. The acquisition of CCR7 by and the subsequent downregulation of CD24 expression on thymocytes mark distinct stages during CD4SP lineage differentiation. Both were reduced in Foxn1$^{wt*/-}$ mice compared to wild type animals revealing a more prominent albeit still partial block in post-selection maturation of CD4SP Foxn1$^{wt*/-}$ mice compared to *Cd83*$^{-/-}$ animals (Fig. 6d).

Discussion

Drawing on newly created mouse models, we identified in postnatal TEC a core set of 450 high confidence Foxn1 target genes that, among other functions, control multiple mechanisms essential for self-antigen processing and presentation. Our findings demonstrate that Foxn1 controls essential functions in TEC biology in addition to those previously noted to be important for initial stages in thymus organogenesis and early thymopoiesis2.

Our *in vivo* ChIP-seq data using nuclear lysates from primary TEC of Foxn1$^{wt*/wt*}$ mice established the Foxn1 consensus binding motif, 5'- a/g/t-G-A-C-G-C, with a core identical to that previously identified by *in vitro* studies16,35. Although our analysis predicted GAAGC as an alternative motif, mutational analyses of the *Psmb11* and *CD83* promoters showed no significant functional contributions of Foxn1 binding to these sequences. However, productive Foxn1 binding to this alternative motif may occur in other cellular or developmental contexts and could depend on co-factors to specify tissue-contextual gene expression profiles as suggested for other Fox family members32,33. Although specific co-factors that physically or functionally associate with Foxn1 have so far not been identified, our ChIP-seq data recognized several transcription factor binding motifs enriched in the vicinity of canonical Foxn1 binding sites, for example those for the transcriptional regulator TP63. An association of Foxn1 with TP63 is intriguing because TP63 maintains TEC stemness34, is positioned upstream of and physically interacts with the PRC1 (polycomb repressive complex) component CBX4, which we identified here as a high confidence Foxn1 target. Interestingly, the lack of *Cbx4* expression impairs TEC generation, proliferation and thymopoietic function35. In this context, it is also noteworthy that *Tbata,* which also controls TEC proliferation36, is another Foxn1 target gene we have identified.

Differences in gene expression profiles between TEC isolated from *Foxn1*$^{nu/nu}$ and wild type mice have previously and by inference been understood to be transcriptionally controlled by Foxn1, including *MHCII*9, *Pax1*9 and *FGFR2*37. However, our data exclude these loci as direct Foxn1 targets (at least in postnatal TEC) and suggest that their transcriptional changes are the indirect consequences of alterations in *Foxn1* complementation. In contrast, our experimental approach combining ChIP-seq and gene expression profiling confirmed the previously suspected targets *Dll4, Cxcl12* and *Ccl25* to be indeed controlled by Foxn1. These findings provide a validated molecular explanation for the failure of *Foxn1*-deficient TEC to attract ETP38 and to assure their subsequent commitment to a T cell fate18.

Importantly, our approach also identified thymic Foxn1 target genes that function at stages beyond the early arrest in thymus organogenesis characteristic for *Foxn1*$^{nu/nu}$ mice and marked by a lack of regular homing of ETP and their commitment to the T cell lineage. Many of these hitherto unrecognized Foxn1 target genes are involved in thymocyte development and selection, with functions extending from self-antigen processing to T cell activation and post-selection maturation. Investigating the function of *Psmb11*- and *Cd83*-deficient TEC, respectively, revealed the most likely molecular cause of some of the major phenotypic features observed in Foxn1$^{wt*/wt*}$ and Foxn1$^{wt*/-}$ mice. However, determining the extent of *Cd83's* and *Psmb11's* contributions to the observed phenotypes will necessitate transgenic reconstitution experiments in Foxn1$^{-/-}$ mice similar to those that established a critical role of the direct Foxn1 targets *Dll4* and *Cxcl12* in early T cell development41. Interestingly, transgenic expression of *Dll4* and *Cxcl12* in *Foxn1*$^{-/-}$ TEC was only sufficient to support thymocyte development up to the DP stage38.

The iFoxn1$^{\Delta 7,8}$ mouse model demonstrated also the need for continuous *Foxn1* expression to maintain regular thymopoietic activity by cTEC. Dox treatment of these mice deleted exons encoding the forkhead and the transcriptional activation domains and resulted in a 2-fold reduction of full length *Foxn1* transcripts within 24 hours and, a decreased expression

of hundreds of cTEC genes within 72 hours (≥ 3-fold: 406 genes; ≥ 2-fold: 1192 genes), affecting total thymocyte cellularity and early thymocyte differentiation at that point in time. Though at variance with a previous observation for reasons yet to be elucidated39, our results clearly demonstrate the importance of continued *Foxn1* expression for the functional competence of post-natal cTEC.

Taken together, our results demonstrate for the first time that *Foxn1* directly binds to and controls the transcription of several hundred genes that, in aggregate, control essential checkpoints during intrathymic T cell development. These genes are critical for the steady-state function of adult TEC and their expression needs to be preserved for the continued thymopoietic competence of the thymus.

Online Methods

Mice

C57BL/6 and *Foxn1*$^{nu/nu}$ mice were obtained from Janvier and Taconic respectively. The generation of β5t-rtTA, and TetO-Cre animals has previously been reported11,40. Mice transgenic for a BAC encoding a Foxn1-Flag fusion protein under the regulatory control of the *Foxn1* locus were generated similarly to the previously reported *Foxn1-Cre* mice11. Foxn1-Flag transgenic mice were subsequently backcrossed onto a *Foxn1*$^{nu/nu}$ background to obtain mice homozygous or heterozygous for the BAC transgene, designated Foxn1$^{wt*/wt*}$ and Foxn1$^{wt*/-}$, respectively. Mice with a conditional *Foxn1* locus where exons 7 and 8 are flanked by loxP sites were generated by homologous recombination, and subsequently crossed to β5t-rtTA and TetO-Cre transgenic animals to obtain triple transgenic mice, designated iFoxn1$^{\Delta 7,8}$. Sex-matched male and female mice aged 4-7 weeks were used. No specific exclusion criteria were used in mouse experiments. All animals were kept under specific pathogen-free conditions and experiments were carried out in accordance with local and national regulations and permissions approved by Kantonales Veterinäramt BS.

Doxycycline Treatment

One week old iFoxn1$^{\Delta 7,8}$ mice were treated with a single intraperitoneal (i.p.) injection of Dox (0.3mg).

Flow Cytometry

Thymocytes were incubated with Abs against TCR beta (1:400, H57-597; Biolegend), CD4 (1:1000, GK1.5; BioLegend), CD5 (1:400, 53-7.3, eBioscience), CD8 (1:500, 53-67; BioLegend), CD25 (1:1000, PC61.5; BioLegend), CD44 (1:500, IM7; BioLegend), c-kit (1:200, 2B8; BioLegend), CD24 (1:1000, M1/69; BioLegend), CD69 (1:200, H1.2F3; BioLegend), PD-1 (1:200, 29F.1A12, Biolegend), CCR7 (1:200, 4B12, BioLegend). For intracellular staining, cells were fixed, permeabilized (Fixation/Permeabilization kit, eBioscience) and stained for Foxp3 (1:70, FJK-16S, eBioscience) and Helios (1:70, 22F6, eBioscience). TECs were stained using Abs against CD45 (1:400, 30F11; BioLegend), EpCAM (1:1000, G8.8; BioLegend), MHCII (1:1000, M5/114.15.2; BioLegend), Ly51 (1:1000, 6C3; BioLegend), UEA-1 (1:1000, Reactolab), CD80 (1:500, 16-10A1, Biolegend), CD86 (1:500, GL-1, Biolegend), CD83 (1:500, Michel 19, Biolegend). For intracellular

staining, cells were fixed, permeabilized (Cytofix/Cytoperm Kit, BD Biosciences) and labelled for the expression of CD83. Stained samples were acquired on a FACSAria II or BD LSRFortessa flow cytometers and the data was analyzed using the FlowJo (Treestar) software.

Quantitative PCR analysis

Total RNA was isolated from sorted cells with the RNeasy Kit (Qiagen), cDNA was synthesized using SuperScriptIII (Live Technologies) and assessed by qPCR (SensiMix; Bioline).

ChIP-seq—Thymic lobes from one week old Foxn1$^{wt*/wt*}$ mice were digested with 0.2mg/ml Liberase TM (Roche Diagnostics) and 30μg/ml DNaseI (Roche Diagnostics) in PBS at 37°C for 30-60 min. TECs were enriched to 15-20% using magnetic beads (autoMACS Pro Separator, Miltenyi Biotech) and then subjected to DNA crosslinking. Nuclear isolation and chromatin fragmentation were performed with 20-30 x 10^6 cells enriched for TEC using the *tru*ChIP High Cell Chromatin Shearing Kit with nonionic Shearing Buffer according to the manufacturer's recommendations (Covaris). Chromatin was immunoprecipitated using the M2 anti-FLAG antibody (F1804; Sigma) with parallel input samples prepared from non-immunoprecipitated chromatin41. To increase the specificity of ChIP-seq analysis, it would have been ideal to include immunoprecipitated chromatin from wild type TEC as negative control but the large amount of material required made this approach infeasible. Precipitated DNA from TEC-enriched (15-20%) and control thymocyte only samples was subjected to qPCR analysis using primers specific to promoter regions of *Psmb11* and *Dll4* (both TEC specific genes) and *Foxp3* (thymocyte specific gene) (Supplementary Fig. 3a). DNA samples from multiple ChIP showing successful enrichment of TEC candidate gene promoters were pooled to generate two replicates (5ng each) for library generation and sequencing. Contaminating adapter sequences were removed from fastq sequences using Trimmomatic (version 0.32). Reads were aligned against the mouse genome (UCSC build mm10) using pre-alignment with BWA (version 0.7.5 with the options -q10 -t4) and final alignment was achieved with Stampy (version 1.0.23 with the options -t4 --bamkeepgoodreads - M)42,43. Peaks were called on deduplicated aligned sequences (paired ChIP and input samples) using MACS2 (version 2.0.10) with a relaxed p-value setting of 0.144. Peaks from replicates were then pooled and analysed using irreproducible discovery rate analysis (IDR < 0.05) (https://sites.google.com/site/anshulkundaje/projects/idr). Peaks were filtered against the ENCODE blacklist regions (https://sites.google.com/site/anshulkundaje/projects/blacklists).

RNA-seq—TECs were enriched as detailed above and then sorted using a FACSAria II (BD Bioscience). RNA was isolated using RNeasy kit (Qiagen) and subjected to sequencing (TrueSeq, BGI). Reads were aligned against the Ensembl transcriptome and genome (GRCm38) using Tophat2 (version 2.0.10). Reads were allocated to protein-coding gene meta-features using Rsubread (requiring both pairs of reads to be aligned and excluding multimapping reads). Exon-level expression data was estimated using BEDtools coverage. Differential expression analysis on genes with at least 1 aligned fragment was conducted using general linear modelling in edgeR, correcting for common, trended and tagwise

dispersion, with additional batch correction for the conditional *Foxn1* knock-out model45. Genes were identified as differentially expressed using the default edgeR threshold (FDR < 0.05).

ATAC-seq—A cell pellet of ~10,000 cTEC was lysed, treated with transposase and DNA tagmented in accordance with a previously published protocol46. Tagmented fragments were amplified by PCR and sequenced using an Illumina MiSeq on 75bp paired end reads. Trimmomatic was used to trim Kmer biases from reads (version 0.32). Fragments were aligned to the mm10 genome using Bowtie2 (version 2.2.3 with the options --no-discordant --no-mixed -X 2000). Read positions were corrected for transposon insertion offset. The significance of differences in coverage between sets of genes was estimated using Wilcoxon rank sum tests. ATAC-seq peaks were called using MACS2 (with the options --nomodel --nolambda --keep-dup all --call-summits; FDR < 0.05). Peaks were screened against blacklisted regions.

Statistical analysis of ChIP-seq and RNA-seq—De novo motif discovery within Foxn1 ChIP-seq peaks was carried out using MEMEChIP on the 200 base-pairs surrounding the peak summit. Background nucleotide content was controlled for using a first-order Markov model. Motif location was identified using FIMO with a threshold of $p < 0.05$ on repeat-masked fasta files using a first-order Markov background. The sequence within 100 bases of each ChIP-seq summit was classified as either containing or not containing a version of each candidate Foxn1 recognition motif. General linear regression, adjusting for GC content within 100 bases of each ChIP-seq summit, was performed to test the predictive power of each motif's presence for the significance score assigned to each summit by MACS2. Central enrichment was tested by permuting the position of motifs within 1kb of peak summit 10,000 times and assessing the number of motifs falling into a 200 base central window. Foxn1 ChIP-seq peaks were scanned for co-factor motifs using PScanChIP and a mixed background24. Genomic enrichment was calculated using GAT with 10,000 randomisations, controlling for GC content and using an appropriate workspace as background. Genomic features were annotated using HOMER. ChIP-seq peaks were allocated to genes using a window of 5kb upstream and 100 bases downstream of the TSS. This gene definition was selected to be comparable to ChIP-seq annotation methods such as GREAT but using greater stringency. To establish whether Foxn1 functioned predominantly as a repressor or activator of transcription, we used BETA to integrate the Foxn1 ChIP-seq peaks and cTEC RNA-seq datasets from iFoxn1$^{\Delta 7,8}$ mice (using default settings)19. We then restricted Foxn1 direct gene targets to those significantly differentially expression in the appropriate direction as a result of Foxn1 deficiency and with a Foxn1 binding site within 5kb upstream or 100 bases downstream of the TSS.

Co-expression analysis—Microarray expression data was downloaded from GSE5692823. This was quantile normalised and a thymic epithelial cell-specific (cTEC, mTEC^{lo} and mTEC^{hi}) signed co-expression network constructed using bidirectional weighted correlation in WGCNA22. The optimal soft threshold power was chosen to achieve $r^2 > 0.9$ for the network. Individual sets of genes were analysed by permutation analysis, controlling for expression deciles. This dataset was also used to generate a list of genes

likely to be primarily driven by non-TEC contaminating thymic stromal cells. To this end, the dataset was screened for genes displaying significant differences on ANOVA testing between TECs and non-TECs, 4-fold higher expression in non-TECs than TECs and an expression level in TECs within the bottom quintile of genes.

Gene ontology analysis—Gene ontology analysis was conducted using DAVID20. All enriched GO terms with Benjamini-Hochberg corrected p-values < 0.05 and > 2-fold enrichment were shown in the relevant figures.

Histological analyses

Frozen thymus tissue sections (8μm) were fixed in acetone and stained using Abs specific for Psmb11 (1:500, PD021, MBL), CD4 (1:200, GK1.5; BioLegend), CK5 (1:500, PRB-160P, Covance), CK8 (1:200, TROMA-1, NICHD supported Hybridoma Bank), ERTR7 (1:50, provided by W. van Ewijk, Netherlands), Foxn1 (1:1000, provided by T. Amagai, Japan) and Aire (1:200, 5H12, eBioscience). Images were acquired using a Zeiss LSM510 (Carl Zeiss).

Luciferase assay

Promoter fragments of *Psmb11* and *Cd83* were subcloned into the pGL4.10(luc2, Promega) reporter plasmid and co-transfected with an expression vector encoding Foxn1 into HEK293 cells using FuGENE HD (Promega). Luciferease activity was measured 24hr later using the Dual-Lucifearase Assay kit (Promega). Motifs were mutated using Q5 Site-Directed Mutagenesis Kit (NEB).

Statistical analyses

Statistical analyses for data presented were performed using Students *t* test (unpaired, two-tailed). $P < 0.05$ was considered significant. The statistical evaluation of the ChIP-seq and RNA-seq data is described in separate statistical analysis section above. The sample size used and estimates of variation within groups were based on published results using similar approaches. No randomization was done for animal studies and investigators were not blinded to experimental group allocations.

Supplementary Material

Refer to Web version on PubMed Central for supplementary material.

Acknowledgements

We thank E. Christen, R. Recinos, A. Offinger, D. Nebenius-Oosthulzen, A. Klewe-Nebenius for excellent technical support, M. Gaio and S. Harris for secretarial assistance. J. Lopez-Rios and M. Osterwalder for help establishing ChIP and provision of plasmids. The authors do not have any conflicts of interest related to this study. This work was supported by grants from the Swiss National Foundation (3100- 68310.02 and 3100-122558 to G.A.H), The Wellcome Trust (105045/Z/14/Z to G.A.H. and C.P.P.; 100643/Z/12/Z to A.H.) and the MRC to C.P.P.).

References

1. Anderson G, Takahama Y. Thymic epithelial cells: working class heroes for T cell development and repertoire selection. Trends Immunol. 2012; 33:256–63. [PubMed: 22591984]

2. Hollander G, et al. Cellular and molecular events during early thymus development. Immunol Rev. 2006; 209:28–46. [PubMed: 16448532]
3. Klein L, Kyewski B, Allen PM, Hogquist Ka. Positive and negative selection of the T cell repertoire: what thymocytes see (and don't see). Nat Rev Immunol. 2014; 14:377–91. [PubMed: 24830344]
4. Stritesky GL, et al. Murine thymic selection quantified using a unique method to capture deleted T cells. Proc Natl Acad Sci USA. 2013; 110:4679–84. [PubMed: 23487759]
5. Nehls M, Pfeifer D, Schorpp M, Hedrich H, Boehm T. New member of the winged-helix protein family disrupted in mouse and rat nude mutations. Nature. 1994; 372:103–107. [PubMed: 7969402]
6. Nehls M, et al. Two genetically separable steps in the differentiation of thymic epithelium. Science. 1996; 272:886–889. [PubMed: 8629026]
7. Bleul CC, et al. Formation of a functional thymus initiated by a postnatal epithelial progenitor cell. Nature. 2006; 441:992–6. [PubMed: 16791198]
8. Cheng L, et al. Postnatal tissue-specific disruption of transcription factor Foxn1 triggers acute thymic atrophy. J Biol Chem. 2010; 285:5836–47. [PubMed: 19955175]
9. Nowell CS, et al. Foxn1 regulates lineage progression in cortical and medullary thymic epithelial cells but is dispensable for medullary sublineage divergence. PLoS Genet. 2011; 7:e1002348. [PubMed: 22072979]
10. Chen L, Xiao S, Manley NR. Foxn1 is required to maintain the postnatal thymic microenvironment in a dosage-sensitive manner. Blood. 2009; 113:567–574. [PubMed: 18978204]
11. Zuklys S, et al. Stabilized beta-catenin in thymic epithelial cells blocks thymus development and function. J Immunol. 2009; 182:2997–3007. [PubMed: 19234195]
12. Zlotoff DA, et al. CCR7 and CCR9 together recruit hematopoietic progenitors to the adult thymus. Blood. 2010; 115:1897–1905. [PubMed: 19965655]
13. Ueno T, et al. CCR7 signals are essential for cortex-medulla migration of developing thymocytes. J Exp Med. 2004; 200:493–505. [PubMed: 15302902]
14. Daley SR, Hu DY, Goodnow CC. Helios marks strongly autoreactive CD4+ T cells in two major waves of thymic deletion distinguished by induction of PD-1 or NF-κB. J Exp Med. 2013; 210:269–85. [PubMed: 23337809]
15. Sansom SN, et al. Population and single-cell genomics reveal the Aire dependency, relief from Polycomb silencing, and distribution of self-antigen expression in thymic epithelia. Genome Res. 2014; 24:1918–31. [PubMed: 25224068]
16. Schlake T, Schorpp M, Nehls M, Boehm T. The nude gene encodes a sequence-specific DNA binding protein with homologs in organisms that lack an anticipatory immune system. Proc Natl Acad Sci U S A. 1997; 94:3842–7. [PubMed: 9108066]
17. Ara T, et al. A Role of CXC Chemokine Ligand 12/Stromal Cell-Derived Factor-1/Pre-B Cell Growth Stimulating Factor and Its Receptor CXCR4 in Fetal and Adult T Cell Development in Vivo. J Immunol. 2003; 170:4649–4655. [PubMed: 12707343]
18. Hozumi K, et al. Delta-like 4 is indispensable in thymic environment specific for T cell development. J Exp Med. 2008; 205:2507–2513. [PubMed: 18824583]
19. Wang S, et al. Target analysis by integration of transcriptome and ChIP-seq data with BETA. Nat Protoc. 2013; 8:2502–15. [PubMed: 24263090]
20. Dennis G, et al. DAVID: Database for Annotation, Visualization, and Integrated Discovery. Genome Biol. 2003; 4:P3. [PubMed: 12734009]
21. Gommeaux J, et al. Thymus-specific serine protease regulates positive selection of a subset of CD4+ thymocytes. Eur J Immunol. 2009; 39:956–64. [PubMed: 19283781]
22. Langfelder P, Horvath S. WGCNA: an R package for weighted correlation network analysis. BMC Bioinformatics. 2008; 9:559. [PubMed: 19114008]
23. Ki S, et al. Global transcriptional profiling reveals distinct functions of thymic stromal subsets and age-related changes during thymic involution. Cell Rep. 2014; 9:402–15. [PubMed: 25284794]
24. Zambelli F, Pesole G, Pavesi G. PscanChIP: Finding over-represented transcription factor-binding site motifs and their correlations in sequences from ChIP-Seq experiments. Nucleic Acids Res. 2013; 41:535–543.

25. Impey S, et al. Defining the CREB regulon: A genome-wide analysis of transcription factor regulatory regions. Cell. 2004; 119:1041–1054. [PubMed: 15620361]
26. Burnley P, et al. Role of the p63-Foxn1 regulatory axis in thymic epithelial cell homeostasis during aging. Cell Death Dis. 2013; 4:e932. [PubMed: 24263106]
27. Gatta, G Della, et al. Direct targets of the TRP63 transcription factor revealed by a combination of gene expression profiling and reverse engineering. Genome Res. 2008; 18:939–948. [PubMed: 18441228]
28. Ripen AM, Nitta T, Murata S, Tanaka K, Takahama Y. Ontogeny of thymic cortical epithelial cells expressing the thymoproteasome subunit β5t. Eur J Immunol. 2011; 41:1278–1287. [PubMed: 21469133]
29. Murata S, et al. Regulation of CD8+ T cell development by thymus-specific proteasomes. Science. 2007; 316:1349–1353. [PubMed: 17540904]
30. Fujimoto Y, et al. CD83 expression influences CD4+ T cell development in the thymus. Cell. 2002; 108:755–767. [PubMed: 11955430]
31. Saini M, et al. Regulation of Zap70 expression during thymocyte development enables temporal separation of CD4 and CD8 repertoire selection at different signaling thresholds. Sci Signal. 2010; 3:ra23. [PubMed: 20332428]
32. Nakagawa S, Gisselbrecht SS, Rogers JM, Hartl DL, Bulyk ML. DNA-binding specificity changes in the evolution of forkhead transcription factors. Proc Natl Acad Sci U S A. 2013; 110:12349–54. [PubMed: 23836653]
33. Carroll JS, et al. Chromosome-wide mapping of estrogen receptor binding reveals long-range regulation requiring the forkhead protein FoxA1. Cell. 2005; 122:33–43. [PubMed: 16009131]
34. Senoo M, Pinto F, Crum CP, McKeon F. p63 Is essential for the proliferative potential of stem cells in stratified epithelia. Cell. 2007; 129:523–36. [PubMed: 17482546]
35. Liu B, et al. Cbx4 regulates the proliferation of thymic epithelial cells and thymus function. Development. 2013; 140:780–8. [PubMed: 23362346]
36. Flomerfelt, Fa, et al. Tbata modulates thymic stromal cell proliferation and thymus function. J Exp Med. 2010; 207:2521–32. [PubMed: 20937703]
37. Bredenkamp N, Nowell CS, Blackburn CC. Regeneration of the aged thymus by a single transcription factor. Development. 2014; 141:1627–1637. [PubMed: 24715454]
38. Calderón L, Boehm T. Synergistic, context-dependent, and hierarchical functions of epithelial components in thymic microenvironments. Cell. 2012; 149:159–172. [PubMed: 22464328]
39. Rode I, et al. Foxn1 Protein Expression in the Developing, Aging, and Regenerating Thymus. J Immunol. 2015; 195:5678–5687. [PubMed: 26538393]
40. Mayer CE, et al. Dynamic spatio-temporal contribution of single beta5t+ cortical epithelial precursors to the thymus medulla. Eur J Immunol. 2016; 46:846–856. [PubMed: 26694097]
41. Vokes, Sa, et al. Genomic characterization of Gli-activator targets in sonic hedgehog-mediated neural patterning. Development. 2007; 134:1977–1989. [PubMed: 17442700]
42. Li H, Durbin R. Fast and accurate short read alignment with Burrows-Wheeler transform. Bioinformatics. 2009; 25:1754–1760. [PubMed: 19451168]
43. Lunter G, Goodson M. Stampy: A statistical algorithm for sensitive and fast mapping of Illumina sequence reads. Genome Res. 2011; 21:936–939. [PubMed: 20980556]
44. Zhang Y, et al. Model-based Analysis of ChIP-Seq (MACS). Genome Biol. 2008; 9
45. Robinson MD, McCarthy DJ, Smyth GK. edgeR: A Bioconductor package for differential expression analysis of digital gene expression data. Bioinformatics. 2009; 26:139–140. [PubMed: 19910308]
46. Buenrostro JD, Wu B, Chang HY, Greenleaf WJ. ATAC-seq: A method for assaying chromatin accessibility genome-wide. Curr Protoc Mol Biol. 2015; 2015:21.29.1–21.29.9. [PubMed: 25559105]

Europe PMC Funders Author Manuscripts

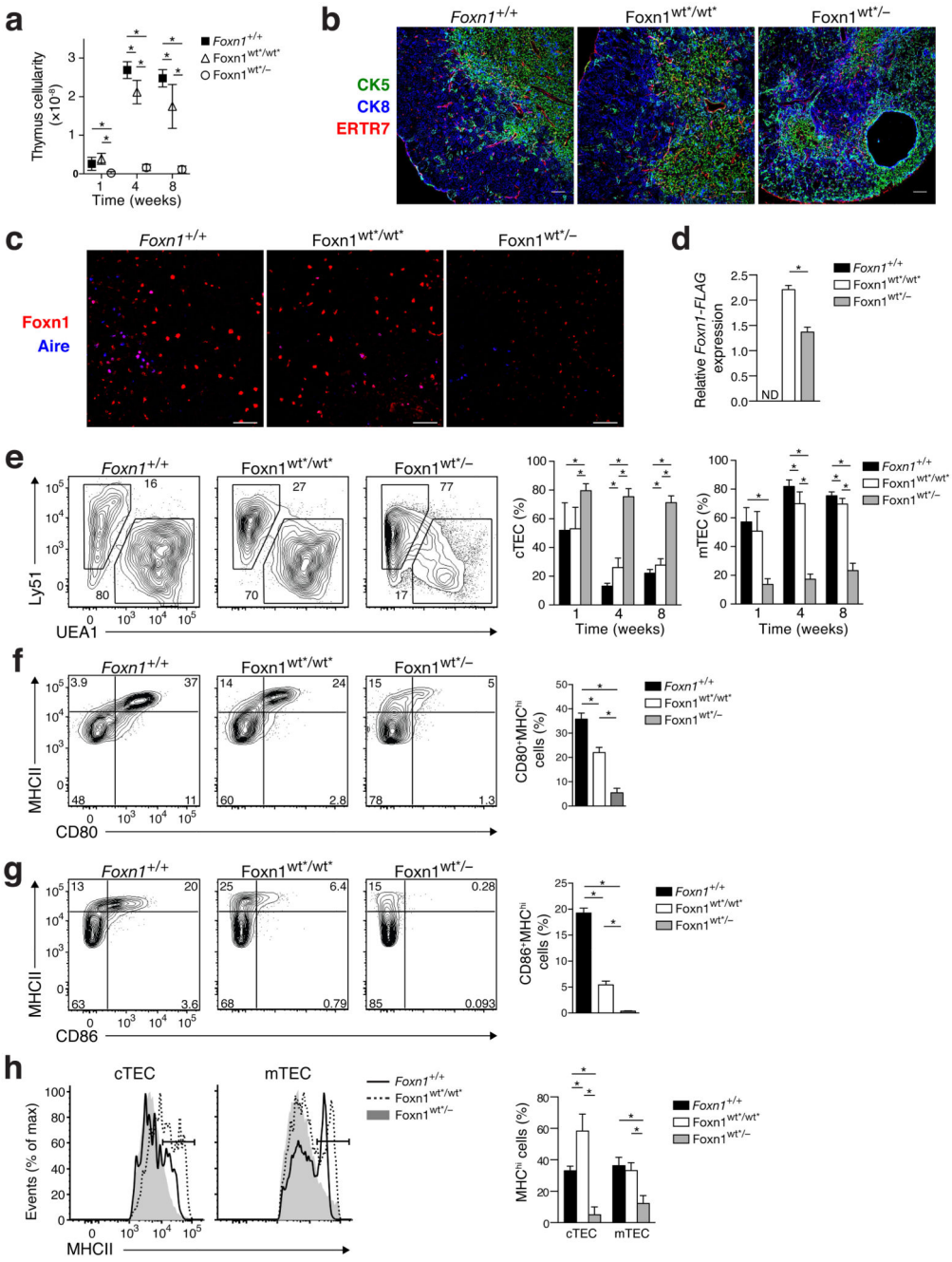

Figure 1.

Transgenic rescue of nude phenotype in Foxn1$^{wt*/wt*}$ mice expressing a chimeric Foxn1-Flag protein. (**a**) Absolute thymus cellularity of mice with indicated genotype and age. (**b, c**) Immunofluorescence analysis of thymus tissue from 4 week old mice with indicated genotype (**b**) for the expression of cytokeratin 8 (CK8; a cortical TEC marker, blue), CK5 (a medullary TEC marker, green), and ERTR7 (endothelial cells and fibroblasts; red), and (**c**) for the expression of Foxn1 (red) and the Autoimmune Regulator (Aire, identifying a subpopulation of mature mTEC; blue). Scale bar 50μm (**c**) and 100μm (**b**). (**d**) RT-qPCR

analysis of functional *Foxn1* transcripts in cTEC from Foxn1$^{wt*/wt*}$ and Foxn1$^{wt*/-}$ mice using oligonucleotides specific for transgene specific FLAG tag sequence. Values are normalized to *EpCAM* expression. (**e**) Flow cytometric analysis of TEC subpopulations isolated from 4 week old mice with the indicated genotype (left panels). The gating strategy is detailed in Supplementary Fig. 1e. Frequencies of cTEC and mTEC in middle and right panels, respectively. (**f,g**) Flow cytometric analysis of mTEC isolated from 4 week old mice mice with the indicated genotype for the expression of MHCII and (**f**) CD80 or (**g**) CD86. Frequencies of double positive cells displayed on the right. (**h**) Flow cytometric analysis of MHCII expression on cTEC and mTEC isolated from 4 week old mice with the indicated genotypes. Bar graph displays frequencies of MHCII^{hi} cells as defined by the gate in the histograms. **p<0.05.* (Student's t-test (**a,d-h**)). Data in bar graphs are pooled from two (**a,e,h**) independent experiments (n=7, mean ±SD) or display one experiment (**b,c,f,g**) representative of two independent experiments with four replicates each. Contour plots (**e-g**) and histograms (**h**) are representative of data in bar graphs. Numbers shown in individual gates and quadrants of flow cytometry plots represent the frequencies observed in a representative experiment. ND: not detected

Europe PMC Funders Author Manuscripts

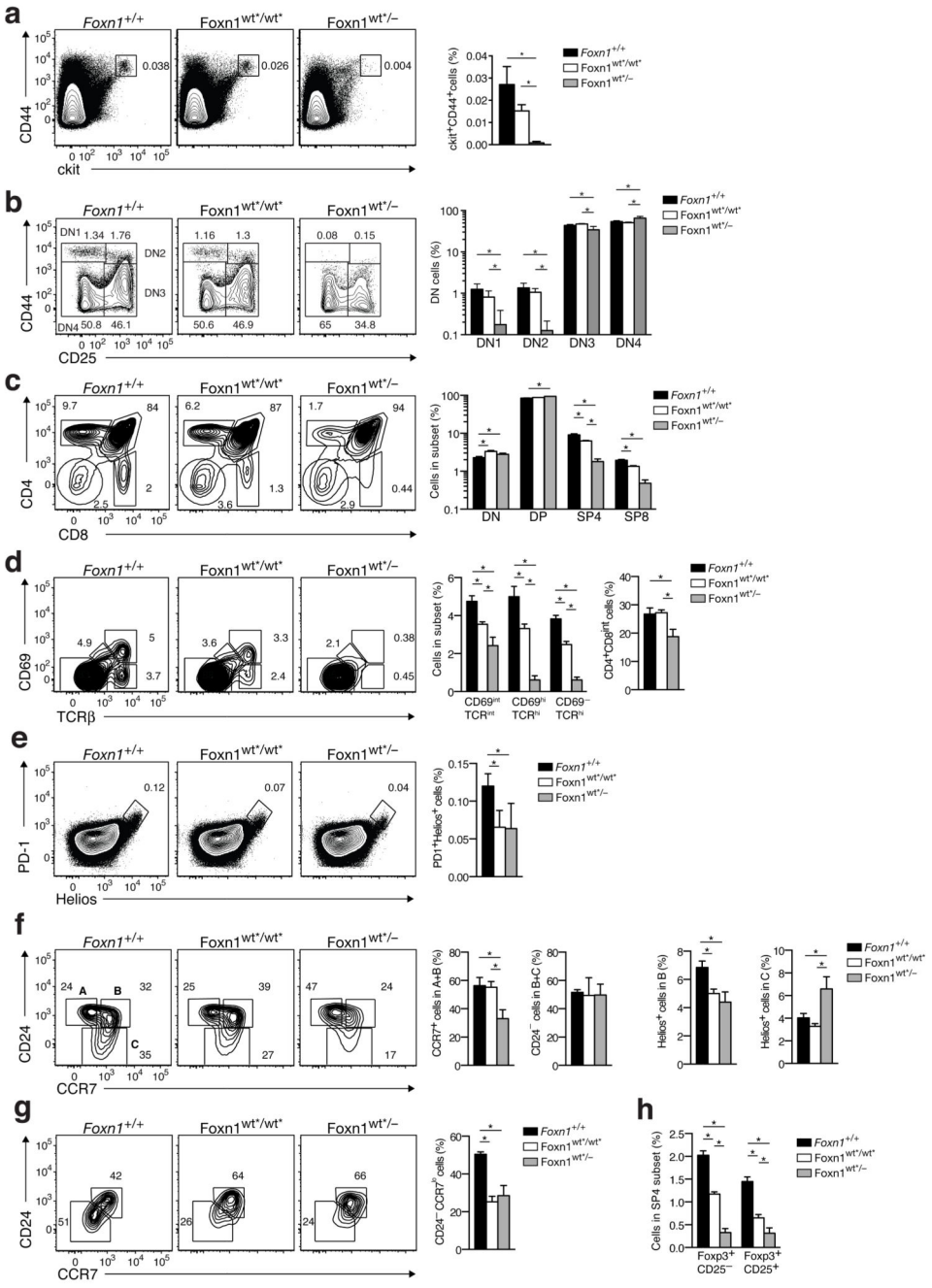

Figure 2.

Foxn1 availability in TEC determines T cell developmental defects. Flow cytometric analysis of 4 week old mice with indicated genotype for (**a**) $CD44^{+}$c-kit^{+} thymocytes. Bar graph display frequencies of $CD44^{+}$c-$kit^{+}CD25^{-}$ thymocytes. (**b**) CD44 and CD25 expression on $CD4^{-}CD8^{-}Lin^{-}$ thymocytes, (**c**) CD4 and CD8 expression on total thymocytes; (**d**) CD69 and TCR β-chain expression on total thymocytes; (**e**) Helios and PD1 expression on $Foxp3^{-}CCR7^{-}$ thymocytes; (**f**) CD24 and CCR7 expression on $CD4^{+}CD8^{-}TCR^{+}CD5^{+}Foxp3^{-}$ thymocytes; (**g**) CD24 and CCR7 expression on

$CD4^{-}CD8^{+}TCR^{+}CD5^{+}$ thymocytes; and (**h**) Foxp3 and CD25 expression by $CD4^{+}CD8^{-}TCR^{+}CD5^{+}$ thymocytes. Representative contour plots for (**h**) are displayed in Supplementary Fig. 2c. **p<0.05.* (Student's t-test (**a-h**). Data in bar graphs are from one experiment representative of two independent experiments with four replicates each. Contour plots (**a-g**) are representative of data in bar graphs. Numbers shown in individual gates and quadrants of flow cytometry plots represent the frequencies observed in a representative experiment.

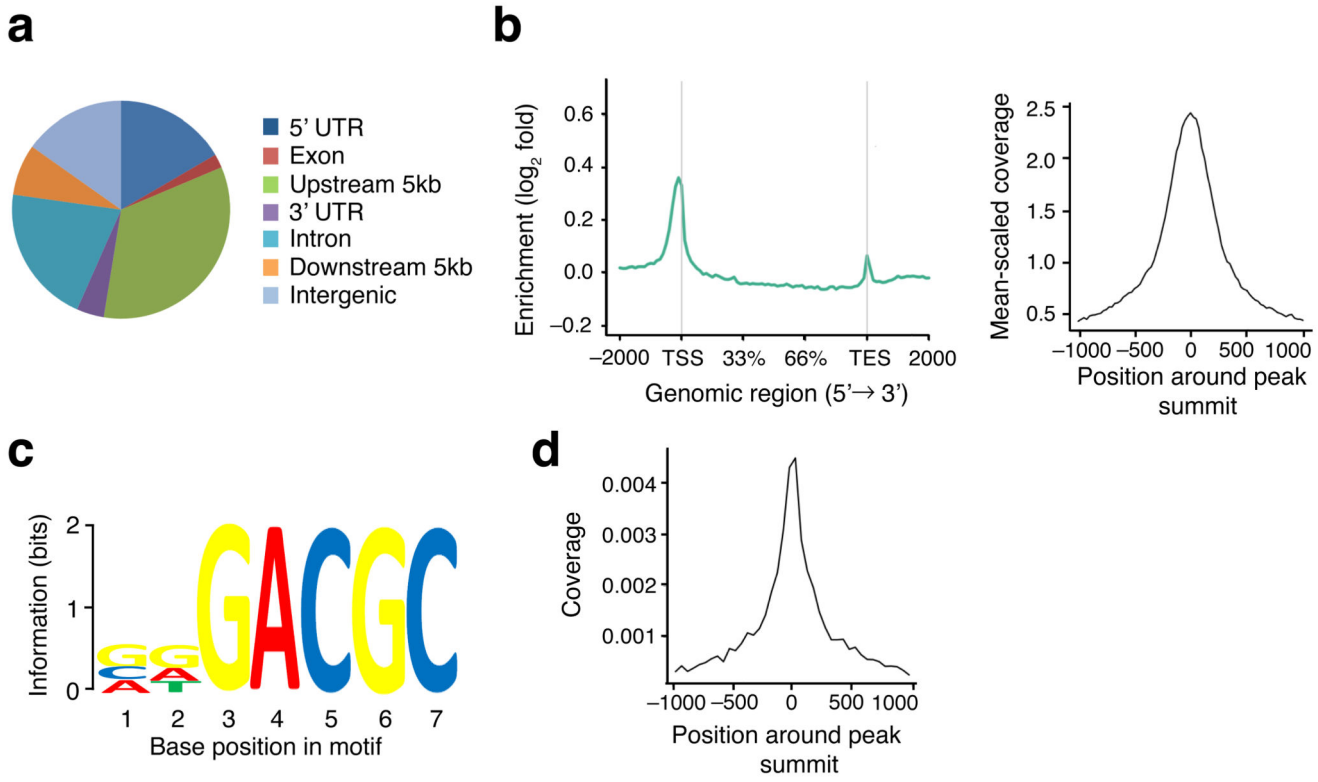

Figure 3.

Foxn1 ChIP-seq analysis. (**a**) Proportion of Foxn1 ChIP-seq peaks falling within different RefSeq meta-gene regions. (**b**) Left: Enrichment of Foxn1 ChIP-seq signal across a meta-gene profile comprising all RefSeq mouse genes relative to control. TSS = transcriptional start site; TES = transcriptional end site. Right: Relative coverage of cTEC ATAC-seq transposon insertions relative to the summit of Foxn1 ChIP-seq peaks. (**c**) MEMEChIP-derived Foxn1 binding site motif for TSS-associated peaks (-5kb before and 100bp after TSS, E-value < 10^{-80}). (**d**) Motif coverage relative to the summit of Foxn1 ChIP-seq peaks for TSS-associated peaks.

Europe PMC Funders Author Manuscripts

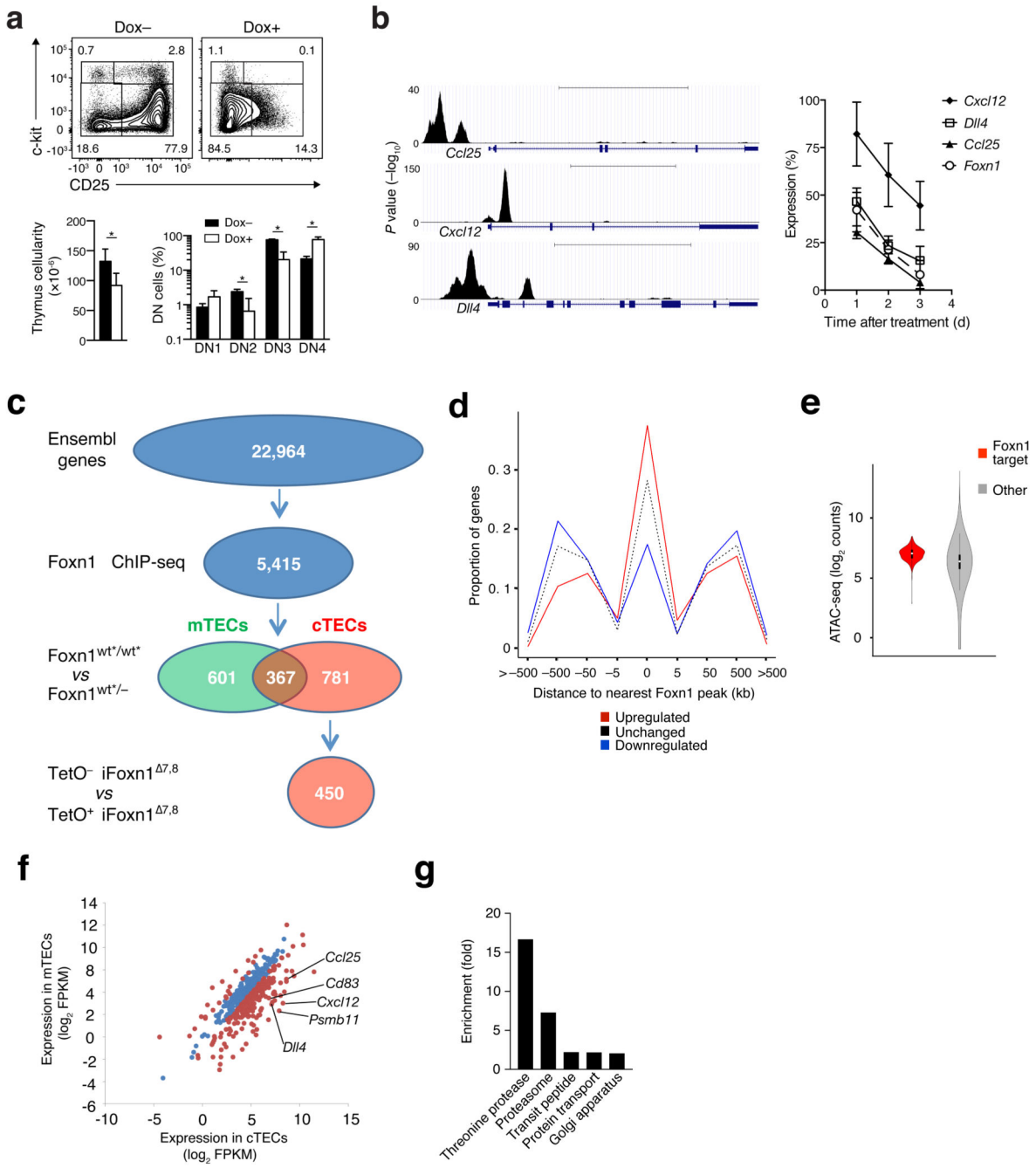

Figure 4.

Intersection of Foxn1 ChIP-seq and RNA-seq analyses. (**a**) Thymus cellularity and expression of c-kit and CD25 on CD4^{-}CD8^{-}Lin^{-} thymocytes in one week old iFoxn1$^{\Delta 7,8}$ mice 72hrs after i.p. exposure to Doxycycline (Dox+) or saline (Dox-). (**b**) Left: Foxn1 ChIP-seq binding profiles for *Ccl25*, *Cxcl12* and *Dll4*. Scale bars represent 5kb (top) and 2kb (middle and bottom). Right: RT-qPCR analysis for *Cxcl12, Dll4, Ccl25* and *Foxn1* transcripts in cTECs isolated at the indicated times after treatment of one week old iFoxn1$^{\Delta 7,8}$ mice with a single dose of Dox relative to untreated iFoxn1$^{\Delta 7,8}$ mice. (**c**) Number

Europe PMC Funders Author Manuscripts

of with decreased Foxn1 activity downregulated genes filtered from all protein coding Ensembl genes by sequential use of indicated data sets. ChIP-seq targets were defined as genes with a Foxn1 peak (IDR < 0.05) 5kb upstream or 100 bases downstream of the TSS. Genes with FDR < 0.05 were called as differentially expressed. (**d**) Distribution of Foxn1 ChIP-seq peaks around the transcriptional start site (TSS) of genes categorized by the direction of change in $TetO^{-}iFoxn1^{\Delta 7,8}$ vs $TetO^{+}iFoxn1^{\Delta 7,8}$ mice following Dox treatment. (**e**) ATAC-seq signal in cTEC near the TSS of high confidence Foxn1 target genes (red) and all other genes (gray; 1.54-median fold change). (**f**) Scatter plot analysis of expression levels of high confidence Foxn1 targets (red: >2-fold; blue: <2-fold differential expression). (**g**) Gene ontology analysis of high confidence Foxn1 gene targets. The number of high confidence targets in each term (> 2 fold enrichment) are: threonine peptidase 8 (representing 38.1% of genes in that gene ontology category); proteasome 9 (16.7%); transit peptides 23 (5.0%); protein trafficking 23 (5.0%) and Golgi apparatus 26 (4.7%). **p<0.05.* (Student's t-test (**a,b**); Benjamini-Hochberg (**g**)).

Europe PMC Funders Author Manuscripts

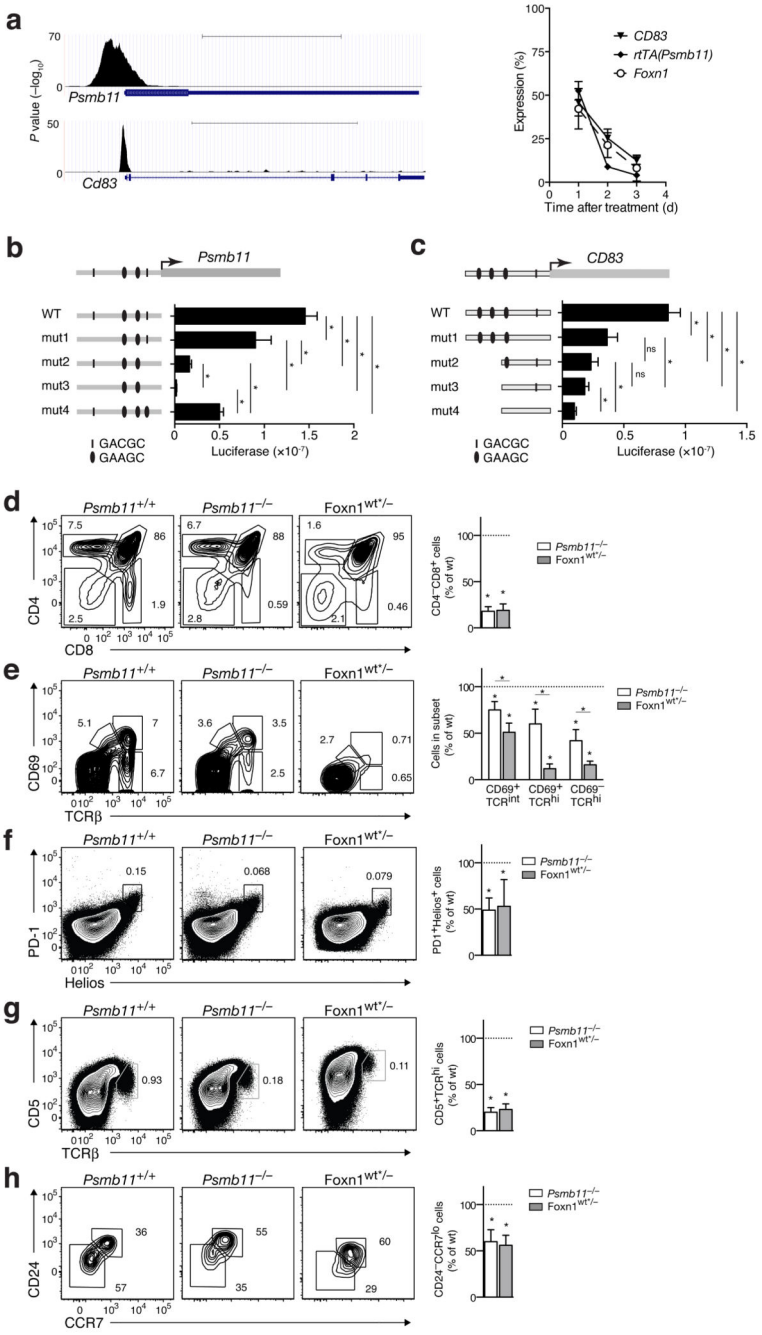

Figure 5.

Psmb11 and *Cd83* are direct targets of Foxn1. (**a**) Left: Foxn1 ChIP-seq binding profiles for *Psmb11* and *Cd83*. Scale bars 2kb (top) and 5kb (bottom). Right: RT-qPCR analysis of gene expression in cTEC isolated from one week old iFoxn1$^{\Delta 7,8}$ mice at the indicated times after treatment with a single dose of Dox relative to untreated iFoxn1$^{\Delta 7,8}$ mice. Measurements of transcripts of the *rtTA* transgene replacing the endogenous *Psmb11* locus in homozygous iFoxn1$^{\Delta 7,8}$ mice. (**b,c**) Luciferase assays for the Foxn1-dependent activation of wild type **(wt)** *Psmb11* and *Cd83* minimal promoters and of *Psmb11* and *Cd83* promoter mutants

(mut1-4) containing alterations in the GACGC (black bars) and GAAGC motifs (black ovals). (**d-h**) Comparative analysis of the impact of a loss of *Psmb11* expression and expression of a hypomorphic *Foxn1* allele, respectively, on intrathymic T cell development of 5 week old mice with indicated genotype for (**d**) CD4 and CD8 expression on thymocytes, (**e**) CD69 and TCR β-chain expression on thymocytes, (**f**) Helios and PD-1 on $Foxp3^{-}CCR7^{-}$ thymocytes, (**g**) CD5 and TCR β-chain expression $CD4^{+}CD8^{+}$ thymocytes, and (**h**) CD24 and CCR7 expression on CD8SP thymocytes. *$*p<0.05$*. (Student's t-test). Data is representative of two independent experiments (mean ±SD) with sample sizes of four (**d-h**) and three measurements each (**a-c**). Contour plots (**d-h**) are representative of data in bar graphs. Numbers shown in individual gates and quadrants of flow cytometry plots represent the frequencies observed in a representative experiment.

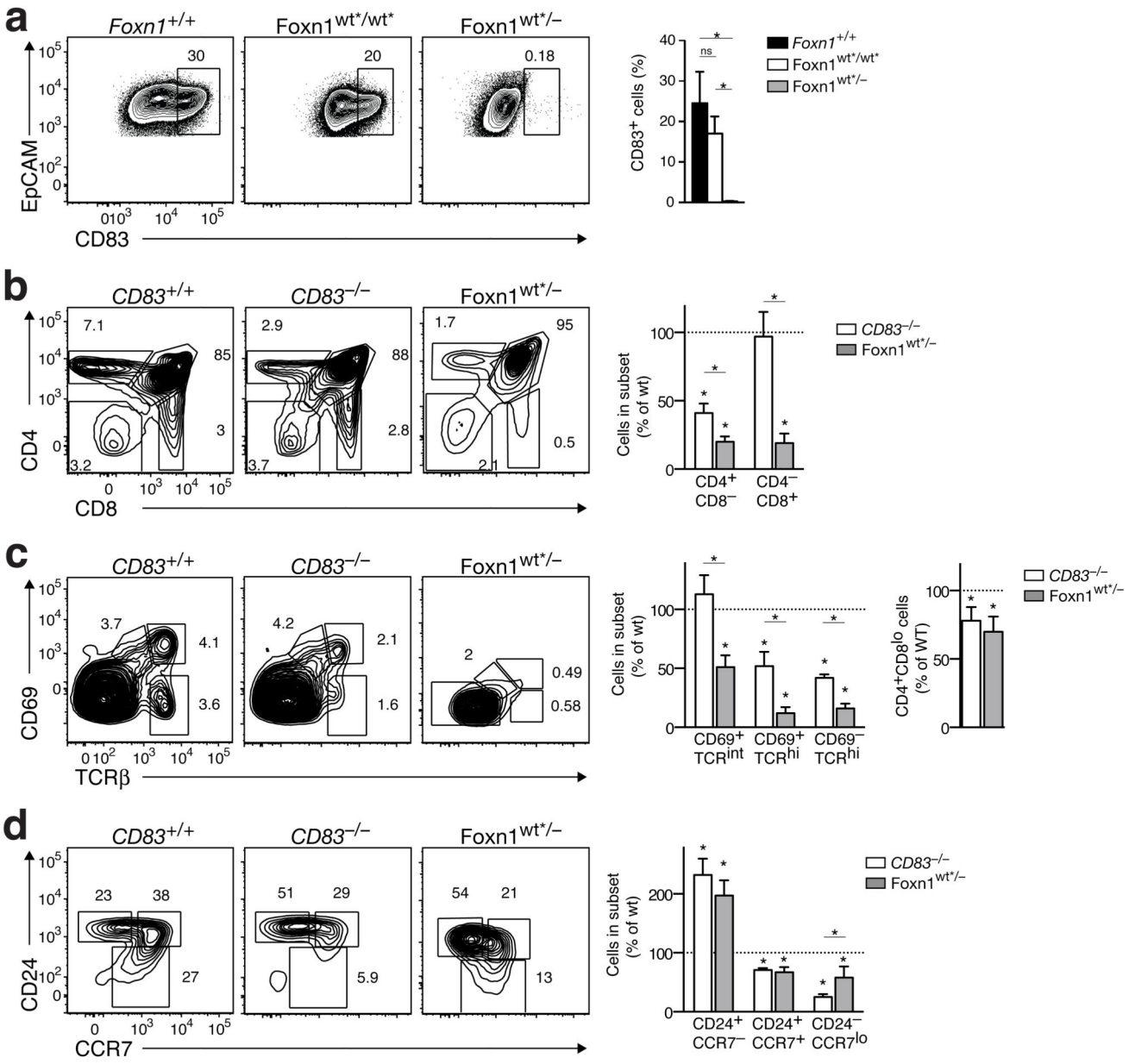

Figure 6.

Comparative analysis of the impact of a loss of *Cd83* expression and expression of a hypomorphic *Foxn1* allele, respectively, on intrathymic T cell development. Analysis of 5 ($Foxn1^{wt*/-}$) and 7 ($Cd83^{+/+}$, $Cd83^{-/-}$) week old mice with indicated genotype for (**a**) EpCAM and CD83 expression on cTEC ($CD45^{-}EpCAM^{+}MHCII^{+}UEA1^{-}Ly51^{+}$), **(b)** CD4 and CD8 expression on total thymocytes, (**c**) CD69 and TCR β-chain expression on total thymocytes, (**d**) CD24 and CCR7 expression on CD4SP thymocytes. *$p<0.05$. (Student's t-test (**a-d**). Data in bar graphs is representative of two independent experiments (mean ±SD) with sample sizes of three. Contour plots are representative of data in bar graphs. Numbers

shown in individual gates and quadrants of flow cytometry plots represent the frequencies observed in a representative experiment.

Europe PMC Funders Author Manuscripts

Table 1

Top 30 Foxn1 target genes.

Gene symbol	Foxn1$^{wt*/-}$ *vs.* Foxn1$^{wt*/wt*}$ cTEC		TetO^{+} *vs.* TetO^{-} iFoxn1$^{\Delta7,8}$ cTEC	
	Log$_2$ fold change	FDR	Log$_2$ fold change	FDR
Ccl25	7.43	0	3.99	3.4E-35
Prss16	4.77	2.1E-121	3.27	5.88E-31
Gpr25	4.33	4.53E-57	2.59	3.57E-16
Tspan10	4.30	6.76E-10	2.44	2.04E-09
AA467197	4.12	4.01E-38	2.55	3.51E-16
Cd83	3.99	5.9E-191	2.75	4.42E-28
Tbata	3.70	1.6E-189	3.88	4.65E-31
Ajap1	3.29	1.34E-67	2.35	1.5E-24
5031414D18Rik	3.27	1.84E-41	2.47	1.97E-16
Psmb11	3.25	2.4E-280	1.67	0.005563
Apba2	3.20	2.5E-199	1.09	1.25E-12
Dtx4	3.09	4.54E-95	1.31	1.34E-12
Pds5b	3.08	1.5E-191	1.12	1.29E-10
Stc2	3.06	4.48E-35	1.55	1.35E-06
Zar1	2.98	1.41E-10	2.46	2.8E-08
Snap91	2.98	1E-121	2.36	2.55E-30
Srxn1	2.93	0	1.12	9.63E-11
Ctnna2	2.89	2.85E-24	1.78	3.76E-05
Lhx3	2.78	0.0212	2.34	0.033605
Cecr6	2.73	4.9E-132	2.93	5.55E-20
Ankmy1	2.70	1.66E-19	2.43	9.39E-10
Tmie	2.68	1.85E-70	1.15	3.47E-11
Abca15	2.67	0.00155	2.38	0.005563
Gmfg	2.67	7.93E-12	0.74	0.018435
Arhgef10l	2.66	0	1.33	9.78E-17
Ptprn2	2.60	2.17E-48	2.01	1.72E-12
Lmx1a	2.59	1.18E-11	2.79	7.24E-06
Endou	2.55	6.52E-14	0.86	0.001829
Mfsd12	2.45	5.7E-217	2.10	2.2E-25
Akap2	2.29	1.27E-25	0.82	0.014184

Top 30 high confidence Foxn1 regulated genes ranked by log2 fold change. High confidence genes (FDR<0.05) are those with a Foxn1 ChIP-seq peak 5kb upstream or 100 bases downstream of the transcription start site, and down-regulated in cTEC of Foxn1$^{wt*/-}$ mice relative to cTEC of Foxn1$^{wt*/wt*}$ mice and cTEC from Dox treated iFoxn1$^{\Delta7,8}$ mice mice relative to Dox treated iFoxn1$^{\Delta7,8}$ mice lacking the *TetO-Cre* transgene. Positive fold change indicates higher expression in Foxn1$^{wt*/-}$ mice compared to Foxn1$^{wt*/wt*}$ mice or Dox treated iFoxn1$^{\Delta7,8}$ mice mice relative to Dox treated iFoxn1$^{\Delta7,8}$ mice lacking the *TetO-Cre* transgene.